Journal of
Composites Science

MDPI

Article

Mesoscopic Simulation on Centrifugal Melt Electrospinning of Polyetherimide and Polyarylethernitrile

Han Guo [1], Yuzhe Huang [1], Jia Chen [1], Hongyu Huo [2], Gongqiu Peng [2], Baoyan Zhang [2] and Yong Liu [1,*]

[1] College of Materials Science and Engineering, Beijing University of Chemical Technology, Beijing 100029, China
[2] AVIC Composite Materials Co., Ltd., Shunyi District Aviation Industrial Park, Beijing 101300, China
* Correspondence: yongliu@mail.buct.edu.cn

Abstract: Polyetherimide (PEI) and polyarylethernitrile (PEN) are high–performance materials for various applications. By optimizing their fiber morphology, their performance can be further enhanced, leading to an expanded range of applications in carbon fiber composites. However, developing processes for stable and efficient fiber production remains challenging. This research aims to simulate the preparation of high–performance ultrafine PEI or PEN fibers using electrospinning. A mesoscopic simulation model for centrifugal melt electrospinning was constructed to compare and analyze the changes in molecular chain orientation, unfolding, fiber diameter, and fiber yield under high-voltage electrostatic fields. The simulation results showed that temperature and electric field force had a particular impact on the diameter and yield of PEI and PEN fibers. Changes in rotational speed had negligible effects on both PEI and PEN fibers. Additionally, due to their different molecular structures, PEI and PEN, which have different chain lengths, exhibit varied spinning trends. This study established a mesoscopic dynamic foundation for producing high-performance ultrafine fibers and provided theoretical guidance for future electrospinning experiments.

Keywords: carbon fiber composites; molecular chain orientation; rotational speed; fiber morphology; interlayer toughening

Citation: Guo, H.; Huang, Y.; Chen, J.; Huo, H.; Peng, G.; Zhang, B.; Liu, Y. Mesoscopic Simulation on Centrifugal Melt Electrospinning of Polyetherimide and Polyarylethernitrile. *J. Compos. Sci.* **2024**, *8*, 480. https://doi.org/10.3390/jcs8110480

Academic Editor: Sebastian Schmeer

Received: 11 October 2024
Revised: 30 October 2024
Accepted: 15 November 2024
Published: 19 November 2024

1. Introduction

Polyetherimide (PEI) is a high-performance polymer characterized by flexible ether bonds along its main chain [1,2], contributing to its recyclability. This material exhibits a transparent appearance with an amber coloration. Incorporating an aromatic imine structure in the molecular chain enhances PEI's properties, including high rigidity, hardness, creep resistance, and heat resistance [3–6]. Moreover, ether bonds impart excellent processability and performance to PEI by making the molecular chain flexible [7–9]. The composition of PEI, as depicted in Figure 1, is represented by its structural formula. Notably, PEI possesses a high glass transition temperature and inherent flame retardancy. It shows exceptional mechanical properties, high temperature, and chemical corrosion resistance [10–12]. These distinctive characteristics make PEI highly suitable for various applications, especially in the interlayer toughening of carbon fiber/epoxy resin composite [13–15]. Due to its excellent thermal stability, mechanical strength, and processing performance, the PEI has been applied to the interlaminar toughening of the carbon fiber composites, the mode I initial fracture toughness (G_{IC}) increased by about 28%, and the mode I fracture toughness increased to approximately 3 kJ/m^2 for mode II (G_{IIC}) [16].

Both solution electrospinning and melt electrospinning are potential options for fabricating PEI fibers. However, when exposed to solvents such as chloroform, dimethylformamide, dichloromethane, and N-methylpyrrolidone, PEI's mechanical and thermal properties are significantly compromised. The primary drawback of PEI lies in its poor solvent resistance, which limits its application range [17]. Compared to other high-performance

polymers like polyimide and polyether ether ketone, which require processing temperatures of 400 °C, PEI can be melted and processed at a lower temperature of 340 °C due to its flexible ether and isopropenyl bonds [18,19], which reduces costs and polymer degradation. Hence, the centrifugal melt electrospinning process is suitable for preparing PEI ultrafine fibers. Melt electrospinning expands the application range by avoiding any negative effects on PEI's performance caused by solvents.

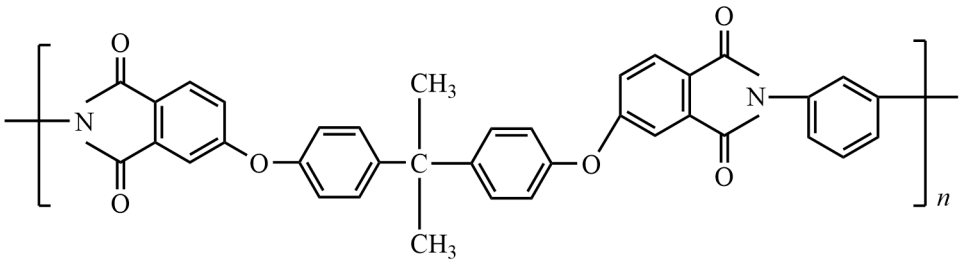

Figure 1. Schematic diagram of the molecular structure of PEI.

Polyarylene ether nitrile (PEN) is a polymer that incorporates aryl, ether, and cyano side chains. The structural formula of PEN is depicted in Figure 2, where Ar represents diverse aromatic binary phenols, such as bisphenol A, resorcinol, and hexafluorobisphenol A [20–22]. Benzene ring structures along the main chain of PEN molecules impart exceptional heat resistance, mechanical stability, corrosion resistance, and other desirable properties [23–25]. Including ether bonds on the main chain of polyarylene nitrile enhances its flexibility, facilitating easy molding and processing characteristics. Furthermore, introducing functional cyano groups improves PEN's heat resistance, solubility, and mechanical properties. The cyano groups, serving as potential active sites, undergo reactions with other functional groups under experimental conditions involving heating or metal ion catalysis, enabling functional modifications of PEN [26–28]. The outstanding overall performance of PEN has garnered significant attention in engineering applications, with expectations of its utilization in many fields [29–31].

Unlike the sulfone and ketone groups present in polyethersulfone and polyetheretherketone, the cyano groups in PEN do not appear on the main chain of the molecule but function as side groups to enhance polarity instead. Thus, the flowability is minimally affected, resulting in better melt-state processability. The dipole interactions between the molecular chains are also enhanced, which improves the material's mechanical strength and leads to the enhancement of the bonding between the resin matrix and the filler [32]. Additionally, cyano groups can serve as potential crosslinking points, forming network structures with excellent heat resistance.

The rigid structure and the regular molecular chain of PEN result in PEN's poor solubility [33,34]. It is challenging to dissolve PEN in common polar solvents like water, alcohol, or ketones. Nevertheless, the highly customizable structure of PEN allows for diverse structural variations, thereby providing excellent processing capabilities. The molding and processing techniques commonly employed for PEN include traditional extrusion molding, injection molding, compression molding, and electrospinning. Electrospinning, in particular, offers the advantage of producing non-woven fibers with nanoscale diameters, thereby significantly enhancing the material's mechanical properties [10,35,36], specific surface area, and volume ratio [37,38]. In our previous work, we achieved a 69% increase in G_{IC} by adding PEN membranes into the laminates [32], revealing its potential in the interlayer reinforcing of the carbon fiber composites.

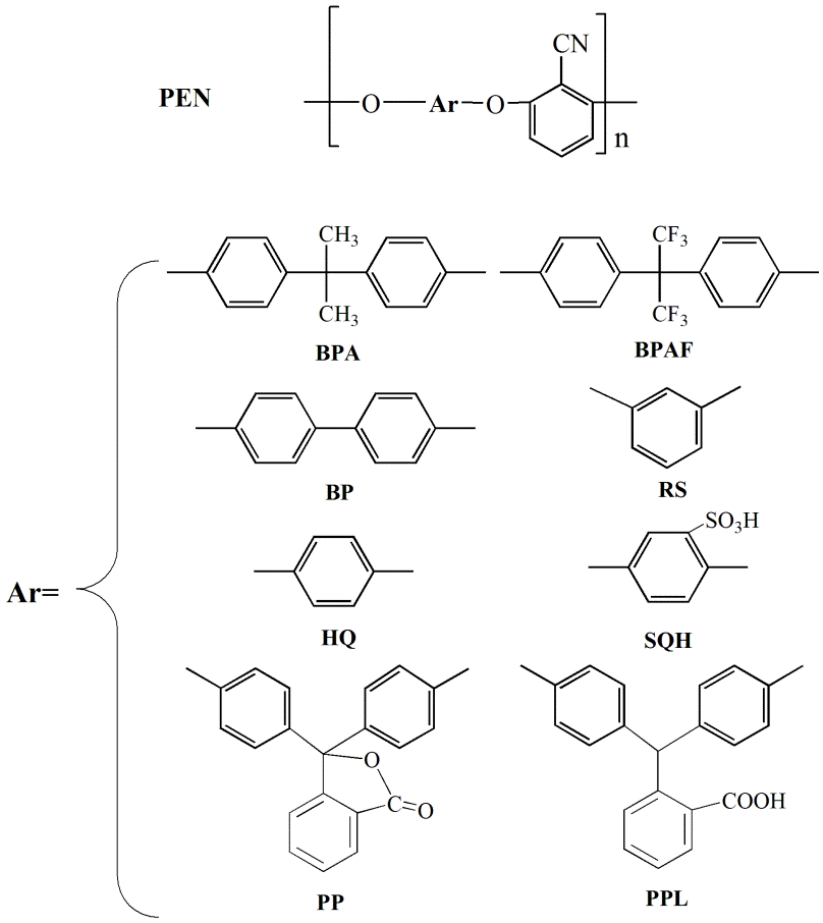

Figure 2. Schematic diagram of the molecular structure of PEN.

Utilizing melt electrospinning to prepare PEI and PEN fibers circumvents the need for solvents, thereby mitigating potential damage to the PEI and PEN materials while concurrently broadening their scope of application. Compared to conventional melt electrospinning, centrifugal melt electrospinning offers advantages such as producing finer fibers, higher production efficiency, solvent-free operation, and environmental friendliness [39–43]. This technique effectively harnesses the exceptional performance of PEI and PEN, thereby enhancing their application value. Before the practical experimental preparation of PEI and PEN fibers through centrifugal melt electrospinning, we hope to gain a better understanding of the differences between the two polymers during the spinning. So, this study created a mesoscopic simulation model for centrifugal melt electrospinning of PEI and PEN, taking into account their molecular structural characteristics. Four key variables that significantly impact the electrospinning effect of polymer melt are considered: electric field strength, rotational speed, temperature, and molecular chain length. Multiple simulations are conducted under each set of variables, and the resulting data are summarized and analyzed to provide theoretical guidance for spinning experiments.

2. Dissipative Particle Dynamics (DPD) Parameters and Model

2.1. DPD Simulation Method

The DPD simulation method, which emerged in the 1990s, is a mesoscale simulation technique that combines molecular dynamics and lattice gas methods [44–46]. Leveraging its strengths in simulating complex fluids, DPD simulation is well-suited for centrifugal melt electrospinning (shown in Figure 3a). In the DPD simulation system, shown in Figure 3b, the fluid particles can be treated as coarse-grained polymer molecules. Furthermore, if the influence of polymer chains is considered, the particles in the system can be

viewed as aggregates of monomeric units, such as chain segments or crystallite. Compared to molecular simulations, DPD provides a dynamic depiction of the spinning process from a mesoscopic perspective while significantly enhancing computational efficiency.

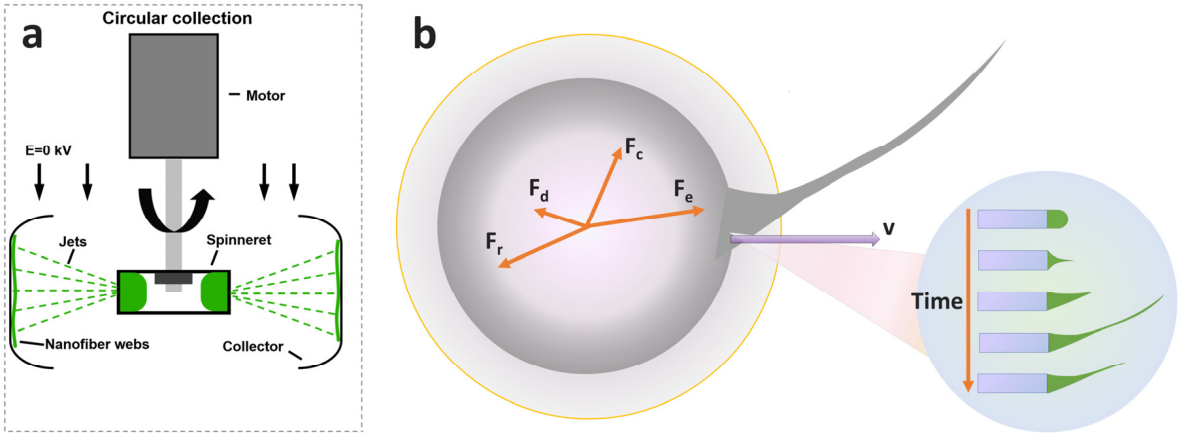

Figure 3. (**a**) Schematic illustration of centrifugal melt Electrospinning system. (**b**) A schematic diagram of centrifugal fiber stress and the fiber formation process, with the right side showing the progression of the jet from initiation to fiber formation.

A detailed analysis of the centrifugal melt electrospinning process is required to establish an appropriate model. During centrifugal melt electrospinning, polymer melts like PEI and PEN are subjected to complex forces, including centrifugal force, electric field force, gravitational force, air resistance, surface tension, and viscous force. These forces act in different planes, and their directions are different. In the fiber stretching process, the centrifugal and electric field forces are the most crucial forces affecting the fiber's trajectory. Among them, the centrifugal force ($\vec{\mathbf{F_c}}$) is the driving force for the circular motion of the jet and is related to the angular velocity ($\vec{\mathbf{\Omega}}$). The calculation formula is presented in the Equation (1):

$$\vec{\mathbf{F_c}} = 2\mathbf{m}\vec{\mathbf{\Omega}} \times \vec{\mathbf{v}} \tag{1}$$

where $\mathbf{m}$ is the mass of the particle, in this research $\mathbf{m}$ = 1 is assumed, and $\vec{\mathbf{v}}$ represents the absolute velocity of the melt drop.

The electric field force ($\vec{\mathbf{F_e}}$) is the driving force for the radial motion of the jet and is related to the field strength ($\vec{\mathbf{E}}$) and the charge ($\mathbf{q}$), as shown in Equation (2).

$$\vec{\mathbf{F_e}} = \vec{\mathbf{E}}\mathbf{q} \tag{2}$$

$\vec{\mathbf{F_r}}$ is the resistance encountered during the jet motion, including air resistance and internal viscous resistance within the melt. The calculation formula is shown in the Equation (3)

$$\vec{\mathbf{F_r}} = \eta\left(\vec{\mathbf{v}} - \vec{\mathbf{\Omega}} \times \vec{\mathbf{r}}\right) \tag{3}$$

where η is the viscosity factor, $\vec{\mathbf{r}}$ represents the vector of the electric field

The Coriolis force ($\vec{\mathbf{F_d}}$) is determined by the inertia formula of particle motion given in Equation (4).

$$\vec{\mathbf{F_d}} = 2\mathbf{m}\vec{\mathbf{\Omega}} \times \mathbf{v} \tag{4}$$

The four forces above follow Newton's equations of motion, as is shown in Equation (5):

$$\mathbf{m}\frac{\mathbf{d}\vec{\mathbf{v}}}{\mathbf{dt}} = \vec{\mathbf{F}}_{\mathbf{e}} - \vec{\mathbf{F}}_{\mathbf{r}} + \vec{\mathbf{F}}_{\mathbf{c}} - \vec{\mathbf{F}}_{\mathbf{d}} \quad (5)$$

2.2. DPD Parameters and Model

The foundation of DPD simulation lies in the establishment of the system model. In this research, the simulated system comprises 24,000 particles, including 2525 red particles (representing the melt), 2278 yellow particles (representing the turntable), and 19,197 blue particles (representing the air). The initial particle distribution in the system is depicted in Figure 4. In the DPD model, the particles adhere to mass conservation and momentum conservation principles. Within a three-dimensional simulated system, by imposing specified force relationships and constraints on the target particles, the particles undergo intricate force transformations and motion analysis. Position updates over discrete time steps, continuously forming new structural arrangements [47–49]. The computer calculates the force-induced motion of the designated particles. It establishes updated positional coordinates at different time steps to investigate the motion variations in the jet and polymer chains.

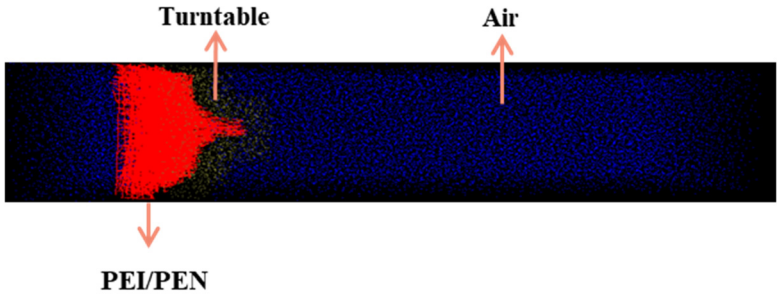

Figure 4. DPD simulation mode of PEI and PEN.

In the set-up program, the red particles were designed to conform to Equations (1)–(5) above. As the jet moves, the coordinates of the particles change, after which the changes in the coordinates of the particles are organized according to the output result file, which in turn analyzes how the jet is affected by different parameters.

The precise methodology for computing the interaction parameters between particles was detailed in the previous work [50,51]. The interaction parameters are determined using χ values, corresponding to the Flory–Huggins parameter for distinct particle types. For particles of the same type, the interaction parameter is denoted as KBT, where KB represents the Boltzmann constant, and T signifies the equilibrium temperature. All values presented in Table 1 are given in KBT units. The calculated results are tabulated, with particles A, B, C, and D representing air, turntable, PEI, and PEN, respectively.

Table 1. The Flory–Huggins parameters χ_{ij} and interaction parameters a_{ij} between particles of PEI and PEN.

Particle Pair	χ_{ij}	a_{ij}
A-B	1.08	28.53
A-C	46.18	176.01
A-D	36.06	142.91
B-C	55.76	207.34
B-D	43.65	167.74

3. Results and Discussion

3.1. Comparative Analysis of the Impact of Rotational Speed

The centrifugal melting electrospinning yield is intricately linked to the centrifugal force and represents a pivotal factor that significantly influences the performance of PEI and PEN fiber [52,53]. Therefore, investigating the impact of rotational speed on the characteristics of PEI and PEN is of utmost importance. In the DPD simulation, a program is designed to set proportional parameters corresponding to different rotational speeds. The visualization software is employed to observe the trajectory of PEI and PEN fibers as they reach the boundary. The changes in PEI and PEN fibers were compared and analyzed.

Figure 5 illustrates the jet trajectories, revealing that the length of the PEI jet reaching the boundary remains relatively constant as the rotational speed increases. In the initial stage, the length of the PEN jet reaching the boundary slightly increases with the rotational speed, but this change becomes insignificant later. Figure 6a demonstrates that the average diameter of both PEI and PEN fibers decreases with the rotational speed increasing. As the speed increases from 10 to 20, the average diameters of PEI and PEN fibers remain within ranges of 11.9–14.6 and 9.8–12.0, respectively. Notably, the decrease in diameter is more pronounced for PEI fibers, which can be attributed to flexible ether bonds in its main chain. The decrease is related to the gradually amplified centrifugal force acting on a jet with a higher rotational speed. Conversely, it can be seen from Figure 6b that as the set speed coefficient increases, the overall trend of PEN fiber production remains relatively stable (205.1–205.9, a 0.3% increase), whereas the yield of PEI fibers decreases from 206.1 to 203.8 (a 1.11% decrease). This can be attributed to the introduction of cyano (–CN) side groups in the molecular chains of PEN, which enhances its mechanical properties and renders it less sensitive to rotational speed. However, the yields of both PEI and PEN fibers are minimally affected by adjustments in rotating speed, suggesting it is not a key factor influencing fiber yield.

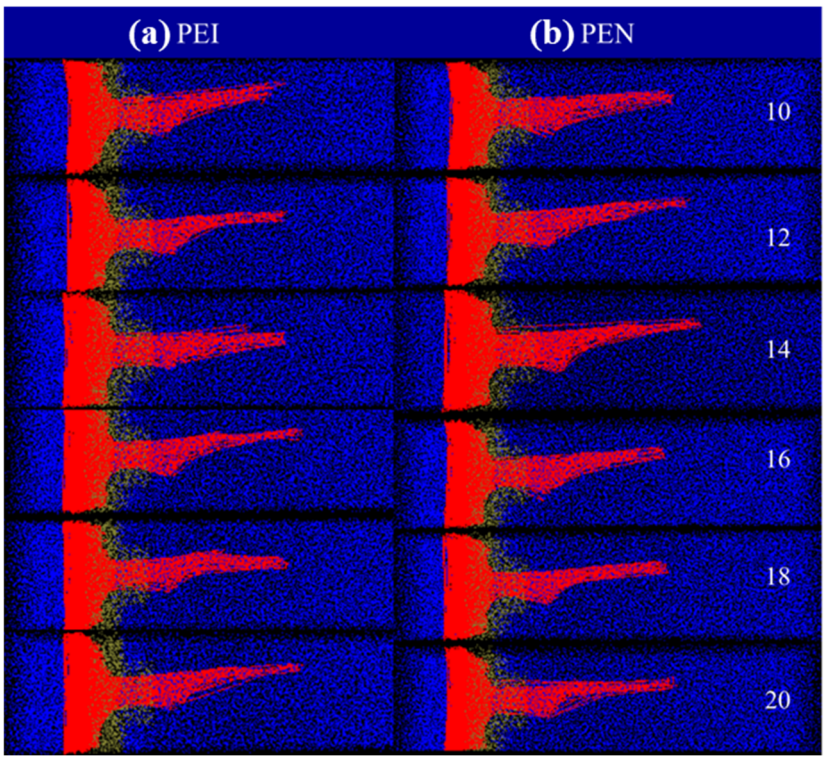

Figure 5. Comparison of descent trajectories of PEI and PEN optical fibers at different rotational speeds.

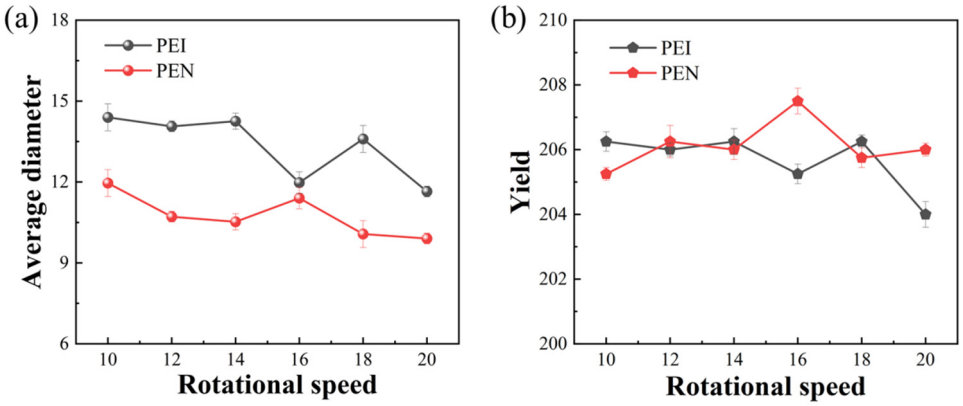

Figure 6. The effect of different rotational speeds on PEI and PEN fiber (**a**) diameter and (**b**) yield.

3.2. Comparative Analysis of the Impact of Temperature

The centrifugal melt electrospinning method uses heating equipment to melt polymers at high temperatures. Under high pressure, the molten polymer is electrostatically stretched to form a polymer jet, which is then collected and solidified to obtain ultrafine filaments. In this context, the heating temperature is crucial as a process parameter affecting the diameter and yield of polymer fibers [54,55]. However, centrifugal melt electrospinning fibers typically exhibit coarser diameters than fibers produced via solution electrospinning [56]. This disparity is primarily attributed to polymer melts' higher viscosity than polymer solutions. Additionally, the polymer is prone to solidify upon being sprayed from the nozzle, which hampers the stretching of the polymer jet. Consequently, it becomes imperative to investigate the influence of temperature on the spinning process.

Different system temperatures are set in the DPD simulation program to investigate their effects. Figure 7 illustrates that the jet's trajectory increases as the system temperature rises, with a more pronounced impact observed for PEN. This behavior can be attributed to numerous rigid benzene rings and flexible ether bond structures in the main chain of PEN, which contribute to its high-temperature resistance and processability. Furthermore, Figure 7 reveals that at a system temperature of 0.16, the PEI jet exhibits a bifurcated structure at the tail. From a simulation perspective, as the system temperature increases, the total kinetic energy of the system rises, indicating heightened activity of PEI particles and increased molecular motion. The particles in the simulation system become disordered, resulting in jet bifurcation. From an experimental perspective, the viscosity of PEI melt decreases with the increase in system temperature, leading to an increase in the fluidity of polymer melt. This phenomenon facilitates the stretching of PEI fibers. It is worth noting that compared to other high-performance polymers, the processing temperature of PEI is lower, usually around 340 °C in industry, which helps to reduce energy costs.

Based on Figure 8a, it is evident that the diameters of both PEN and PEI fibers exhibit a decreasing trend with increasing system temperature, with a more significant reduction observed for PEN in the initial stage. This behavior can be attributed to pendant cyano groups on the molecular chain of PEN, which imparts unique characteristics compared to other specialty polymers. These cyano groups have minimal impact on the flowability during processing and enhance the processability of PEN. Figure 8b shows that the yield of PEI and PEN fibers increases by 39.4% and 36.8%, respectively, with the system temperature rising, demonstrating a significant contrast to the effects of rotational speed. Such a phenomenon can be attributed to the decrease in melt viscosity as the temperature increases, facilitating easier ejection. Within the same time frame, the amount of material expelled from the spinneret gradually increases, offering the possibility of controlling the yield by adjusting the temperature.

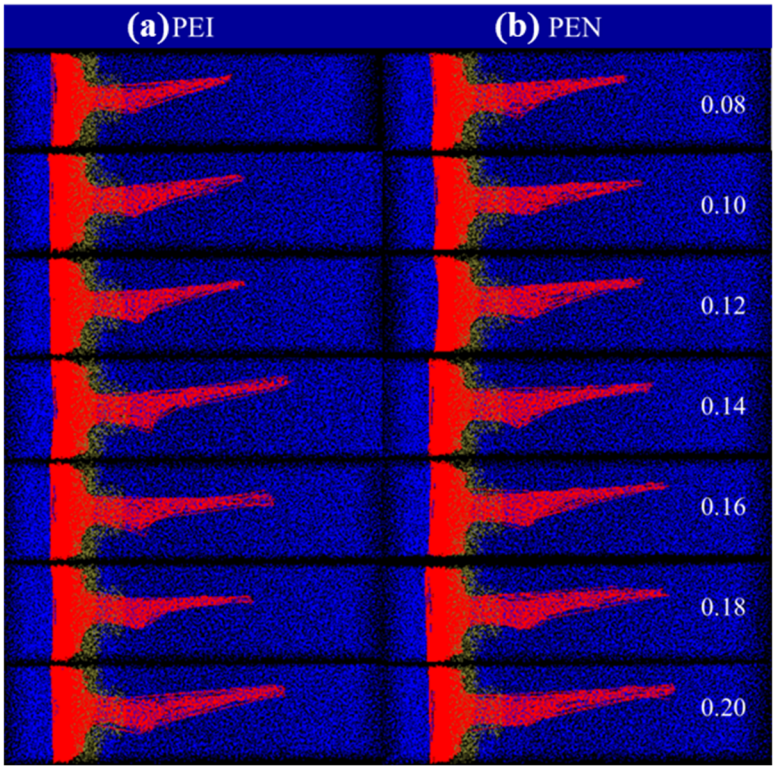

Figure 7. Comparison of descent trajectories of PEI and PEN optical fibers at different temperatures.

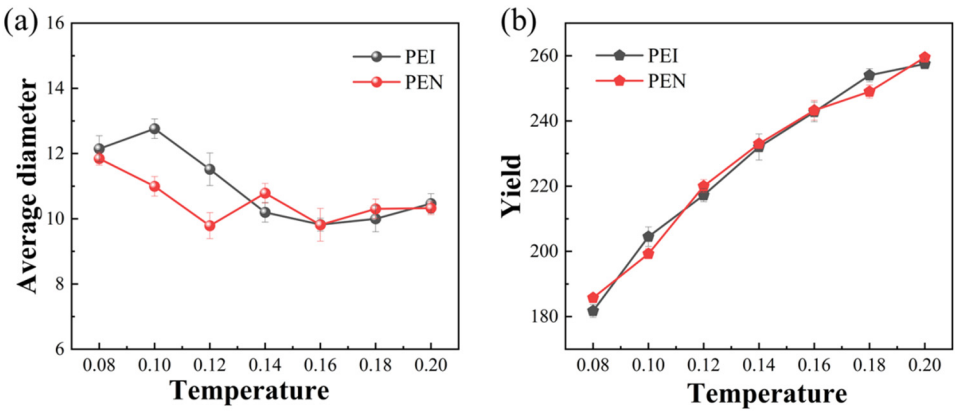

Figure 8. The effect of different temperatures on PEI and PEN fiber (**a**) diameter (**b**) yield.

3.3. Comparative Analysis of the Impact of Electric Field Force

The electric field and temperature are critical factors in fabricating fibers using centrifugal melt electrospinning. The electric field primarily governs the behavior of polymer jets within the rotating region, which plays a key role in reducing the fiber diameter. Applying a high voltage is essential to achieve optimal extension of the electrospinning jet. However, excessively high electric field forces can result in jet instability, excessive elongation, and jet fracture [57–59]. In this study, various electric field force coefficients were employed to observe the motion trajectory of the fiber jet and analyze the impact of different electric field force magnitudes on fiber diameter and yield.

Figure 9 illustrates the trajectories of PEI and PEN fibers under varying electric field forces (in the form of electric field force coefficient). The flight paths of PEI and PEN fibers become longer with increasing electric field force, indicating the significant role of electric field force in achieving complete fiber stretching. In Figure 10a, the diameters of PEI and PEN fibers gradually decrease with the electric field force increasing. With the force becoming stronger, fibers are stretched more intensively, resulting in a higher

length–diameter ratio. The extent of stretching exhibited by PEI fibers (from 25.3 to 11.9, a reduction of 53.0%) is more sensitive to the electric field force, which can be attributed to the unique molecular structure of PEI. The presence of ether bonds in PEI molecular chains imparts a certain degree of flexibility, contributing to its favorable processability. Figure 10b demonstrates that the yield of both PEI and PEN fibers gradually increases with higher electric field force, exceeding a 100% margin and showing a consistent trend. This can be attributed to the fact that both the fibers are pulled toward a high electric field as the electric field force increases.

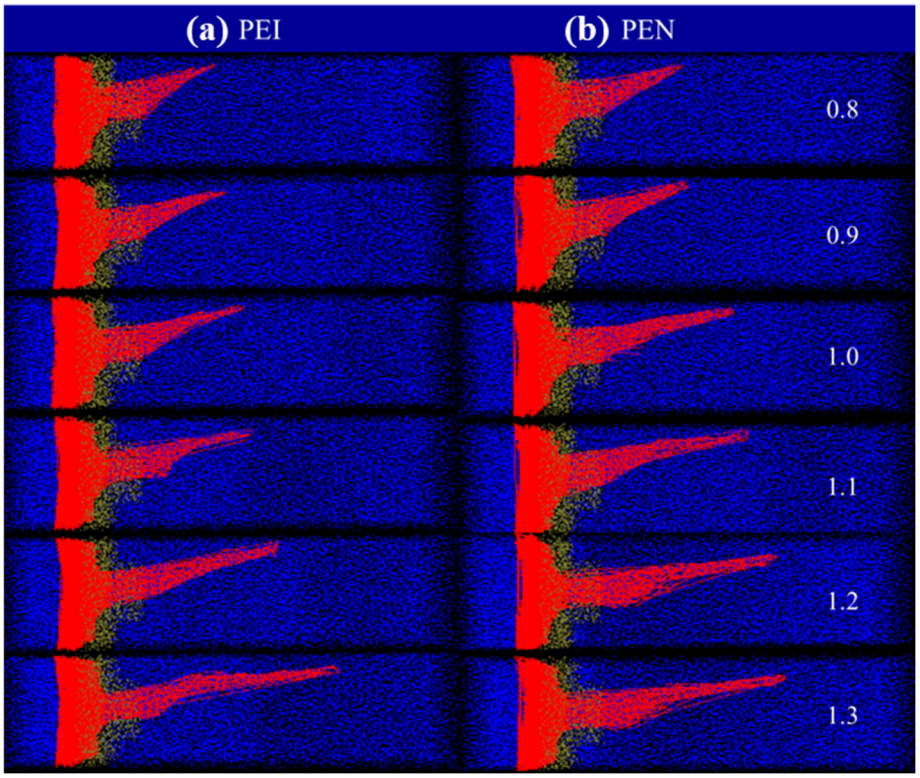

Figure 9. Comparison of descent trajectories of PEI and PEN optical fibers at different electric field forces.

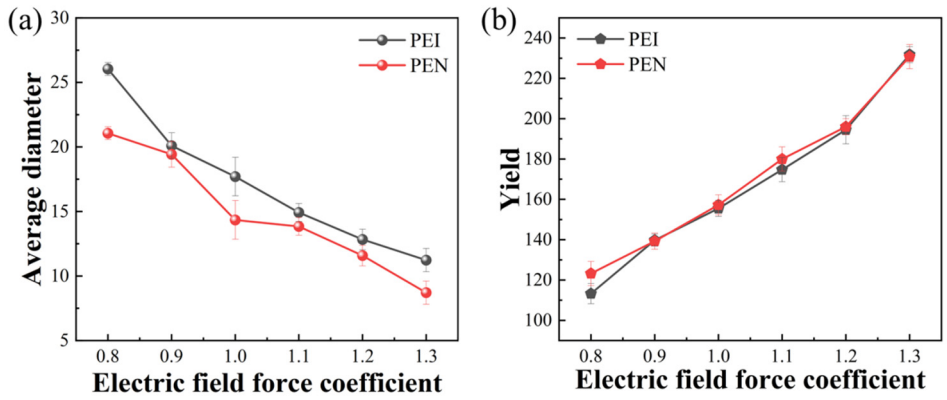

Figure 10. The effect of different electric field forces on PEI and PEN fiber: (**a**) diameter; (**b**) yield.

3.4. Comparative Analysis of the Impact of Molecular Chain Lengths

The length of their molecular chains typically influences polymers' thermal and mechanical properties [60–62]. A simulation model was employed to investigate the effect of different molecular chain lengths on the challenges encountered in centrifugal melt electrospinning experiments. In this model, the molecular weight or relative molecular mass

change was represented by altering the number of bonds connecting the model particles, corresponding to the chain length. The impact of different molecular chain lengths on fiber diameter, yield, and molecular chain entanglement was analyzed by simulating PEI and PEN with various chain lengths.

The spinning process of PEI and PEN with varying molecular chain lengths was simulated, and the diameter of the fibers collected on the receiving plate was calculated. The average diameter was determined by conducting multiple simulations with different lengths for each molecular chain. The results are presented in Figures 11 and 12a. Figure 12a illustrates that the average diameter of both PEI and PEN fibers decreases in the initial stages of molecular chain length variation, with a more pronounced decrease observed in PEI fibers. When the chain length is 2, the molecule is insufficient for producing fibers with a significant relative molecular weight. However, the simulation cannot capture some limitations because the droplet-like fibers may exhibit larger diameters than typical fibers, resulting in diameter fluctuations within the 2–3 chain length range. As the chain length further increases, the average diameter of PEN fibers steadily grows. Attributed to the augmentation of the chain length, more entangled nodes form, resulting from more unfolding, releasing, and sliding of the molecular chains. Consequently, the internal structure becomes more stable, leading to thicker individual fiber diameters.

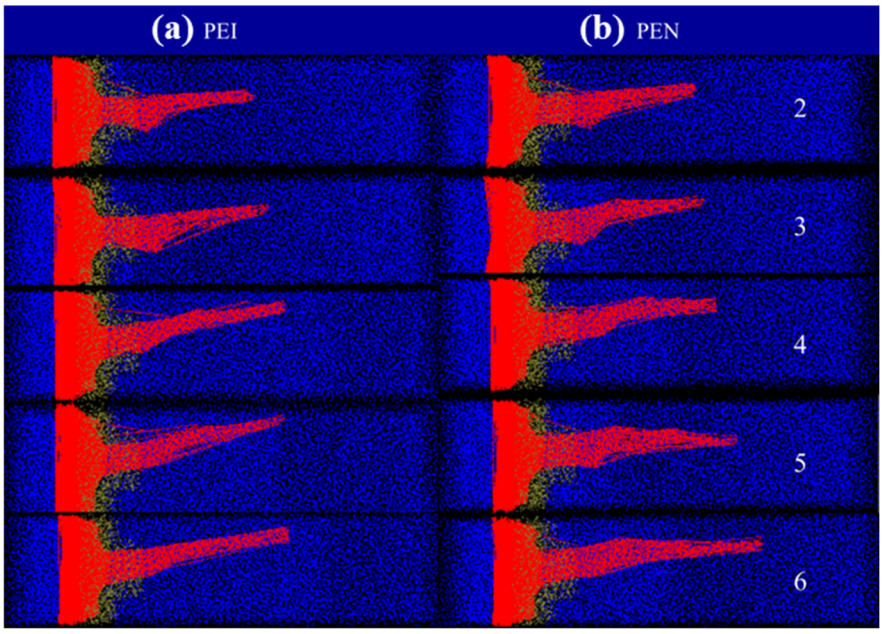

Figure 11. Comparison of descent trajectories of PEI and PEN optical fibers at different molecular chain lengths.

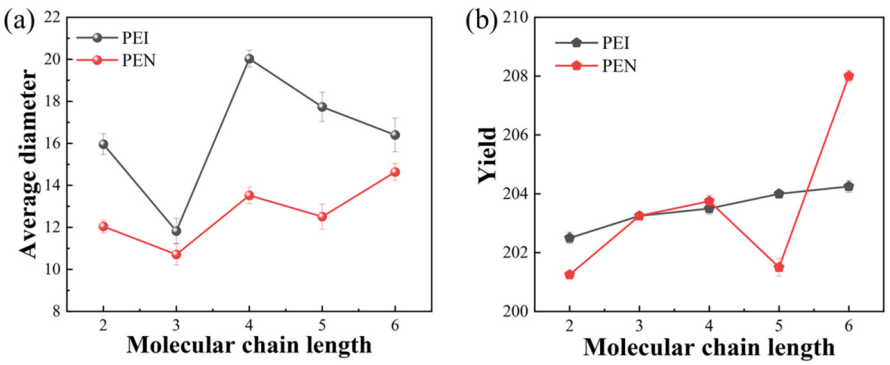

Figure 12. The effect of different molecular chain lengths on PEI and PEN fiber: (**a**) diameter; (**b**) yield.

For PEI fibers, the diameter initially increases and then decreases as the chain length ranges from 3 to 6, which is associated with the molecular structure of PEI. Flexible ether bonds on PEI's main chain effectively reduce intermolecular forces and steric hindrance, enhancing flowability and processability. In Figure 12b, the yield of PEI fibers does not exhibit significant changes with increasing molecular chain length, consistently within the range of 202–204, showing only a slight variation in fiber yield as the relative molecular weight of PEI increases. The time and energy required for melt flow increase, leading to decreased fiber orientation and increased spinning difficulty. Alternatively, the fiber yield increases as the molecular chain length of PEN fibers increases. This may be attributed to the interaction between side cyano groups of PEN, which enhances interchain interactions, improving mechanical properties and material bonding ability. Consequently, polymer chains tend to aggregate into larger structures over a given time, leading to increased diameter and yield.

4. Conclusions

This article employs the DPD method to establish a centrifugal melt electrospinning model for PEI and PEN, considering their distinct molecular structures and setting various parameters for simulation analysis. Among the factors influencing the spinning process of PEI and PEN, temperature is closely associated with the polymer's melting state and serves as a prerequisite for centrifugal melt electrospinning. The electric field force significantly impacts the electrospinning process, while the rotational speed influences the centrifugal force, thereby also affecting the process. Moreover, the molecular chain lengths of PEI and PEN play a crucial role in fiber performance, exhibiting distinct patterns of variation. A comparative analysis was conducted on the parameters affecting the melt electrospinning process, including the diameter, productivity, and jet trajectory simulation of PEI and PEN fibers. The simulation results indicate that increasing the temperature and electric field force within a specific range can refine PEI and PEN fibers and improve fiber yield. It is worth noting that changes in rotational speed have minimal effects on PEI and PEN fibers in the present simulation system. Due to their different molecular structures, PEI and PEN with varying chain lengths show different change trends. In the initial stage, the average diameter of both PEI and PEN fibers decreases, with PEI experiencing a more significant reduction. However, in the later stage, the average diameter of PEN fibers continues to increase, while the diameter of PEI fibers first increases and then decreases. The yield of PEN fibers tends to increase with an increase in molecular chains, whereas the yield of PEI fibers does not show significant changes with the rise in molecular chains.

This study conducted a comparative analysis of the centrifugal melt electrospinning process of PEI and PEN, thereby providing essential theoretical guidance for the development of more reliable techniques to produce future high-quality and functional fibers of PEI and PEN. Through the investigation conducted in this study, researchers can broaden their research horizons and explore novel methodologies within this field.

Author Contributions: Conceptualization, Y.L.; Formal analysis, H.G.; Funding acquisition, B.Z. and Y.L.; Investigation, H.G.; Project administration, G.P., B.Z. and Y.L.; Resources, H.H.; Software, J.C.; Supervision, Y.L.; Validation, Y.H.; Writing—original draft, H.G.; Writing—review and editing, Y.H. and Y.L. All authors have read and agreed to the published version of the manuscript.

Funding: This research was funded by the program 62502510602 of the Aviation Industry Corporation of China, Ltd.

Data Availability Statement: The raw data supporting the conclusions of this article will be made available by the authors upon request.

Acknowledgments: The authors would like to thank Xiaozhen Yang of the Institute of Chemistry, Chinese Academy of Science, for the expert advice in developing this article.

Conflicts of Interest: Author Hongyu Huo, Gongqiu Peng and Baoyan Zhang was employed by the company AVIC Composite Materials Co., Ltd. The remaining authors declare that the research was

conducted in the absence of any commercial or financial relationships that could be construed as a potential conflict of interest.

References

1. Liu, J.; Chen, Z.; Wang, C.; He, J.; Cheng, C.; Li, Q.; Chen, Y.; Bai, L.; Duan, C.; Tang, L.; et al. Functionalizing the surface of polyetherimide (PEI)-based cross-linked separator by introducing the polyamide layer through interfacial polymerization and adding boric acid as electrolyte additive for boosted performance in lithium-oxygen battery. *J. Energy Storage* **2024**, *82*, 110594. [CrossRef]
2. Liu, Z.; Yang, M.; Wang, Z.; Zhao, Y.; Wang, W.; Dang, Z.-M. Simultaneous Inhibition of Conduction Loss and Enhancement of Polarization Intensity of Polyetherimide Dielectrics for High-Temperature Capacitive Energy Storage. *J. Phys. Chem. Lett.* **2023**, *14*, 11550–11557. [CrossRef] [PubMed]
3. Zhang, Y.Y.; Guan, B.W.; Liang, S.W.; Liu, Q.X.; Li, Y.Q.; Fu, S.Y. Frictional and wear behaviors of short carbon fiber reinforced polyetherimide composites in an oil lubricant environment. *Wear* **2024**, *542–543*, 205275. [CrossRef]
4. Wang, J.; Nie, L.; Zhang, C.; Wang, B. Free radical graft polymerization of hydroxyethyl methacrylate and acrylic acid on polyetherimide membrane surface via redox system to improve anti-fouling and oil resistance performance. *Mater. Today Commun.* **2024**, *38*, 108197. [CrossRef]
5. Wan, B.; Yang, X.; Dong, X.; Zheng, M.S.; Zhao, Q.; Zhang, H.; Chen, G.; Zha, J.-W. Dynamic Sustainable Polyimide Film Combining Hardness with Softness via a "Mimosa-Like" Bionic Strategy. *Adv. Mater.* **2023**, *35*, 2207451. [CrossRef]
6. Wan, B.; Dong, X.; Yang, X.; Wang, J.; Zheng, M.S.; Dang, Z.-M.; Chen, G.; Zha, J.-W. Rising of Dynamic Polyimide Materials: A Versatile Dielectric for Electrical and Electronic Applications. *Adv. Mater.* **2023**, *35*, 2301185. [CrossRef]
7. Vidović, N.; Antić, V. Schwarzbauer, Simultaneous identification and quantification of three water-soluble polymers (PVP, PNVCL and PEI) in wastewater samples by continuous-flow off-line pyrolysis GC/MS. *J. Sci. Total Environ.* **2024**, *916*, 170320. [CrossRef]
8. Zhu, L.; Zheng, Z.; Xu, W.; Tang, Y.; Yao, H.; Zhang, Y.; Jiang, Z. Optimizing high-temperature capacitive energy storage performance by constructing crosslinked structure in self-crosslinkable polyetherimides. *Mater. Today Energy* **2022**, *30*, 101145. [CrossRef]
9. Liu, X.-J.; Zheng, M.-S.; Chen, G.; Dang, Z.-M.; Zha, J.-W. High-temperature polyimide dielectric materials for energy storage: Theory, design, preparation and properties. *Energy Environ. Sci.* **2022**, *15*, 56. [CrossRef]
10. Blythe, A.; Fox, B.; Nikzad, M.; Eisenbart, B.; Chai, B.X. Stiffness Retention in Cyclic-Loaded CFRP Composites Produced via Novel Automatic Tape Laying. *J. Compos. Sci.* **2024**, *8*, 92. [CrossRef]
11. Li, C.; Yuan, L.; Liang, G.; Gu, A. A Molecular Design Strategy to Develop All-Organic Crosslinked Polyetherimide Film with High Discharged Energy Density at 150 °C. *J. Appl. Polym. Sci.* **2024**, *141*, e56218. [CrossRef]
12. Kalayci, E.; Avinc, O. Assessing the Washing Fastness and Environmental Impact of Various Reduction Clearing Processes on High-Performance Polyetherimide (PEI) Fabrics. *Fibers Polym.* **2024**, *25*, 2359–2374. [CrossRef]
13. Hao, Y.; Guo, X.; Li, J.; Wang, H.; Liu, F.; Huang, L.; Sun, H.; Guo, X. Polyhydroxy phenolic resin coated polyetherimide membrane with biomimetic super-hydrophily for high-efficient oil-water separation. *Sep. Purif. Technol.* **2024**, *336*, 126278. [CrossRef]
14. Tan, D.Q.; Wu, X. A case study of high-temperature polyetherimide film capacitor fabrication. *Mater. Today Energy* **2022**, *30*, 101167. [CrossRef]
15. Khanbareh, H.; Hegde, M.; Bijleveld, J.; Van Der Zwaag, S.; Groen, P. Functionally graded ferroelectric polyetherimide composites for high temperature sensing. *J. Mater. Chem. C* **2017**, *5*, 9389–9397. [CrossRef]
16. Wang, J.; Pozegic, T.R.; Xu, Z.; Nigmatullin, R.; Harniman, R.L.; Eichhorn, S.J. Cellulose Nanocrystal-Polyetherimide Hybrid Nanofibrous Interleaves for Enhanced Interlaminar Fracture Toughness of Carbon Fibre/Epoxy Composites. *Compos. Sci. Technol.* **2019**, *182*, 107744. [CrossRef]
17. Xu, Z.; Gehui, L.; Cao, K.; Guo, D.; Serrano, J.; Esker, A.; Liu, G. Solvent-Resistant Self-Crosslinked Poly(ether imide). *Macromolecules* **2021**, *54*, 3405–3412. [CrossRef]
18. Yu, Y.; Wu, Y.; Yuan, Y.; Wang, Y.; Xu, C.; Fang, Y.; Gu, Y.; Liu, P.; Wan, Y.; Wang, L.; et al. TiO_2 nanoparticle embedded PEEKWC/PEI cross-linked ultrafiltration membrane: Improvement in flux and anti-fouling properties. *Chem. Eng. Res. Des.* **2024**, *202*, 480–488. [CrossRef]
19. Ye, H.; Gao, W.; Xu, L. High-temperature energy storage capability of polyetherimide composite incorporated with perovskite quantum dots. *Colloids Surf. A* **2024**, *687*, 133479. [CrossRef]
20. Wang, P.; Liu, X.; Liu, H.; He, X.; Zhang, D.; Chen, J.; Li, Y.; Feng, W.; Jia, K.; Lin, J. Combining aggregation-induced emission and instinct high-performance of polyarylene ether nitriles via end-capping with tetraphenylethene. *Eur. Polym. J.* **2022**, *162*, 110916. [CrossRef]
21. Qi, Q.; Qin, J.; Zhang, R.; Luo, S.; Liu, X.; Park, C.B.; Lei, Y. Mechanically robust and thermally insulating polyarylene ether nitrile with a bone-like structure. *Mater. Des.* **2020**, *196*, 109099. [CrossRef]
22. Wang, L.; Bai, Z.; Liu, C.; Wei, R.; Liu, X. Porous fluorinated polyarylene ether nitrile as ultralow permittivity dielectrics used under humid environment. *J. Mater. Chem. C* **2021**, *9*, 860. [CrossRef]
23. Wang, L.; Liu, X.; Liu, C.; Zhou, X.; Liu, C.; Cheng, M.; Wei, R.; Liu, X. Ultralow dielectric constant polyarylene ether nitrile foam with excellent mechanical properties. *Chem. Eng. J.* **2020**, *384*, 123231. [CrossRef]

24. Wei, R.; Tu, L.; You, Y.; Zhan, C.; Wang, Y.; Liu, X. Fabrication of crosslinked single-component polyarylene ether nitrile composite with enhanced dielectric properties. *Polymer* **2019**, *161*, 162. [CrossRef]
25. Wei, R.-B.; Zhan, C.-H.; Yang, Y.; He, P.-L.; Liu, X.-B. Polyarylene ether nitrile and titanium dioxide hybrids as thermal resistant dielectrics. *Chin. J. Polym. Sci.* **2021**, *39*, 211. [CrossRef]
26. Zuo, L.; Li, K.; Ren, D.; Xu, M.; Tong, L.; Liu, X. Surface modification of aramid fiber by crystalline polyarylene ether nitrile sizing for improving interfacial adhesion with polyarylene ether nitrile. *Compos. Part B* **2021**, *217*, 108917. [CrossRef]
27. He, L.; Tong, L.; Xia, Y.; Lin, G.; Wang, T.; Zhang, W.; Liu, Y.; Liu, X. Advanced composites based on end-capped polyarylene ether nitrile/bisphthalonitrile with controllable thermal curing reaction. *Polymer* **2022**, *245*, 124695. [CrossRef]
28. Wang, P.; Liu, X.; Wang, D.; Wang, M.; Zhang, D.; Chen, J.; Li, K.; Li, Y.; Jia, K.; Wang, Z. Recent progress on the poly (arylene ether) s-based electrospun nanofibers for high-performance applications. *Mater. Res. Express* **2021**, *8*, 122003. [CrossRef]
29. Chen, S.; Chen, S.; Lan, J.; Qin, H.; Yang, S.; Wang, P.; You, Y. Core-shell structure polydopamine and polyethylenimine co-assisted MoS_2-$BaTiO_3$/polyarylene ether nitrile nanocomposites for high-temperature resistant organic dielectrics. *J. Alloys Compd.* **2024**, *977*, 173336. [CrossRef]
30. Zhu, J.; Mo, C.; Tong, L.; Liu, X. Synthesis and Properties of Semicrystalline Poly (ether nitrile ketone) Copolymers. *Polymers* **2024**, *16*, 251. [CrossRef]
31. Qin, J.; Tong, L.; He, L.; Liu, X.; Tang, X. Lightweight and high-strength polyarylene ether nitrile-based composites for efficient electromagnetic interference shielding. *Nanotechnol. Rev.* **2023**, *12*, 20230167. [CrossRef]
32. Lv, X.; Huang, Y.; Zhang, B.; Peng, G.; Huo, H.; Qu, X.; Guo, H.; Liu, Y. Electrospun poly (arylene ether nitrile) fibers for interlaminar toughening of carbon fiber epoxy composites. *Polym. Test.* **2024**, *130*, 108299. [CrossRef]
33. Zhang, R.; He, X.; Jia, K.; Liu, X. Facile fabrication of silver decorated polyarylene ether nitrile composited micro/nanospheres via microemulsion self-assembling. *Compos. Part B* **2019**, *156*, 399–405. [CrossRef]
34. Ding, W.; Peng, X.; Li, J.; Heng, Z.; Zhou, S.; Zou, H. Comparative study on the tribological properties of poly (arylene ether nitrile)/polytetrafluoroethylene composites: The influence of filler size and testing conditions. *J. Appl. Polym. Sci.* **2024**, *141*, 54794. [CrossRef]
35. Ji, D.; Lin, Y.; Guo, X.; Ramasubramanian, B.; Wang, R.; Radacsi, N.; Jose, R.; Qin, X.; Ramakrishna, S. Electrospinning of nanofibers. *Nat. Rev. Methods Primers* **2024**, *4*, 1. [CrossRef]
36. Mishra, R.K.; Mishra, P.; Verma, K.; Mondal, A.; Chaudhary, R.G.; Abolhasani, M.M.; Loganathan, S. Electrospinning production of nanofibrous membranes. *Environ. Chem. Lett.* **2019**, *17*, 767–800. [CrossRef]
37. Wang, Y.; Qu, M.; Wang, X.; Zhou, G. Enhanced thermal conductivity of poly (aryl ether nitrile ketone)/functionalized boron nitride composites by electrospinning–hot press technique. *J. Appl. Polym. Sci.* **2022**, *139*, 52399. [CrossRef]
38. Wang, Y.; Qu, M.; Wang, Z.; Wang, S.; Zhou, G. Improving thermal conductivity of poly(aryl ether nitrile ketone) composites by incorporating functionalized boron nitride and silicon carbide via electrospinning-hot press method. *J. Polym. Res.* **2023**, *30*, 80. [CrossRef]
39. Opálková, Š.A.; Petra, P.; Eckstein, A.A.; Igor, J.; Piotr, R. Circulatory Management of Polymer Waste: Recycling into Fine Fibers and Their Applications. *Materials* **2021**, *14*, 4694. [CrossRef]
40. Soukarie, D.; Nocete, L.; Bittner, A.M.; Santiago, I. DNA data storage in electrospun and melt-electrowritten composite nucleic acid-polymer fibers. *Mater. Today Bio* **2024**, *24*, 100900. [CrossRef]
41. Zhang, L.-H.; Duan, X.-P.; Yan, X.; Yu, M.; Ning, X.; Zhao, Y.; Long, Y.-Z. Recent advances in melt electrospinning. *RSC Adv.* **2016**, *6*, 53400. [CrossRef]
42. Yang, Y.; Zheng, N.; Zhou, Y.; Shan, W.; Shen, J. Mechanistic study on rapid fabrication of fibrous films via centrifugal melt spinning. *Int. J. Pharm.* **2019**, *560*, 155. [CrossRef] [PubMed]
43. Molina, A.; Vyas, P.; Khlystov, N.; Kumar, S.; Kothari, A.; Deriso, D.; Liu, Z.; Banavar, S.; Flaum, E.; Prakash, M. Low cost centrifugal melt spinning for distributed manufacturing of non-woven media. *PLoS ONE* **2022**, *17*, 0264933. [CrossRef] [PubMed]
44. Ramin, Z.; Alireza, E.; Moslem, S. DPD simulation of the reciprocating translocation behaviour of polymer chain in a microchannel under variable external force. *Mol. Simul.* **2023**, *49*, 1061.
45. Hoogerbrugge, P.; Koelman, J. Simulating microscopic hydrodynamic phenomena with dissipative particle dynamics. *Europhys. Lett.* **1992**, *19*, 155. [CrossRef]
46. Espanol, P.; Warren, P. Statistical mechanics of dissipative particle dynamics. *Europhys. Lett.* **1995**, *30*, 191. [CrossRef]
47. Sokhan, V.P.; Todorov, I.T. Dissipative particle dynamics: Dissipative forces from atomistic simulation. *Mol. Simul.* **2021**, *47*, 248. [CrossRef]
48. Li, K.; Xu, Y.; Liu, Y.; Mohideen, M.M.; He, H.; Ramakrishna, S. Dissipative particle dynamics simulations of centrifugal melt electrospinning. *J. Mater. Sci.* **2019**, *54*, 9958–9968. [CrossRef]
49. Kumar, P.; Jana, S.; Shyam, H.; Dalal, I.S. Effectiveness of DPD Simulations to Predict the Dynamics of Polymer Chains in Solutions at Equilibrium and Steady Shear Flows. *Macromol. Theory Simul.* **2023**, *32*, 2300045. [CrossRef]
50. Guo, H.; Chen, J.; Lv, X.; Qu, X.; Zhang, B.; Peng, G.; Liu, Y. Mesoscopic Simulation of Centrifugal Melt Electrospinning of PPESK. *Macromol. Theory Simul.* **2023**, *32*, 2300036. [CrossRef]
51. Wang, J.; Xu, Z.; Chen, J.; Yang, X.; Ramakrishna, S.; Liu, Y. Mesoscale simulation on the hydrated morphologies of SPEEK membrane. *Macromol. Theory Simul.* **2021**, *30*, 2100006. [CrossRef]

52. Chen, J.; Yu, Z.; Li, C.; Lv, Y.; Hong, S.; Hu, P.; Liu, Y. Review of the principles, devices, parameters, and applications for centrifugal electrospinning. *Macromol. Mater. Eng.* **2022**, *307*, 2200057. [CrossRef]
53. Chen, J.; Hu, H.; Song, T.; Hong, S.; Li, Y.V.; Wang, C.; Hu, P.; Liu, Y. Competitive effects of centrifugal force and electric field force on centrifugal electrospinning. *Iran. Polym. J.* **2022**, *31*, 1147. [CrossRef]
54. Mu, X.; Zheng, Y.; Li, X.; Xin, B.; Lin, L. Effects of temperature on melt electrospinning: Experiment and simulation study. *Fibers Polym.* **2021**, *22*, 964. [CrossRef]
55. Ge, C.; Zheng, Y.; Liu, K.; Xin, B. Effects of temperature on melt electrospinning with auxiliary heating: Experiment and simulation study. *Text. Res. J.* **2022**, *92*, 1578. [CrossRef]
56. Bachs-Herrera, A.; Yousefzade, O.; del Valle, L.J.; Puiggali, J. Melt Electrospinning of Polymers: Blends, Nanocomposites, Additives and Applications. *Appl. Sci.* **2021**, *11*, 1808. [CrossRef]
57. Chris, V.; Jan, V.; Naveen, R.; Pieter, S.; Jan, D.H.; Roos, P.; Anitha, E.; Mieke, B. Fabrication of poly(3-hydroxybutyrate-co-3-hydroxyhexanoate) Fibers Using Centrifugal Fiber Spinning: Structure, Properties and Application Potential. *Polymers* **2023**, *15*, 1181. [CrossRef]
58. Li, X.; Zheng, Y.; Mu, X.; Xin, B.; Lin, L. Jet motion and fiber properties arising from a parallel electric field in melt-electrospinning. *Text. Res. J.* **2021**, *91*, 899. [CrossRef]
59. Radoor, S.; Karayil, J.; Jayakumar, A.; Siengchin, S. Efficient removal of dyes, heavy metals and oil-water from wastewater using electrospun nanofiber membranes: A review. *J. Water Process Eng.* **2024**, *59*, 104983. [CrossRef]
60. Li, W.; Zhu, Z.; Yang, J. Effect of grafting density and side chain length on the mechanical properties of comb polymers under shear flow: Insights from molecular dynamic simulations. *Comput. Mater. Sci.* **2024**, *235*, 112812.
61. Yang, H.; Cai, Z.; Liu, H.; Cao, Z.; Xia, Y.; Ma, W.; Gong, F.; Tao, G.; Liu, C. Tailoring the surface of attapulgite by combining redox-initiated RAFT polymerization with alkynyl-thiol click reaction for polycarbonate nanocomposites: Effect of polymer brush chain length on mechanical, thermal and rheological properties. *Mater. Chem. Phys.* **2020**, *241*, 122334. [CrossRef]
62. Lin, E.Y.; Frischknecht, A.L.; Winey, K.I.; Riggleman, R.A. Effect of surface properties and polymer chain length on polymer adsorption in solution. *J. Chem. Phy.* **2021**, *155*, 034701. [CrossRef] [PubMed]